Eur. Phys. J. D **29**, 209–216 (2004)
DOI: 10.1140/epjd/e2004-00031-5

THE EUROPEAN PHYSICAL JOURNAL D

Off-shell effects in laser-assisted scattering

S. Hokland[a] and L.B. Madsen[b]

Department of Physics and Astronomy, University of Aarhus, 8000 Århus C, Denmark

Received 18 December 2003 / Received in final form 20 January 2004
Published online 9 March 2004 –

Abstract. We present calculations of laser-assisted differential cross-sections in the second Born approximation. We explore effects of off-the-energy-shell propagation, and we conclude, contrary to other works, that this effect, although significant when compared to the second Born on-shell approximation, is too small for the second Born approximation to account for experimental results.

PACS. 34.80.Qb Laser-modified scattering – 34.50.Rk Laser-modified scattering and reactions

1 Introduction

In laser-assisted scattering, collision events in the presence of a laser field are explored. The special case of a 'free-free' process, where the target atom is assumed to be unaffected by the collision, and the projectile electron is assumed to be 'free' before and after the collision event, may be described schematically as [atomic units will be used throughout unless otherwise stated]

$$e_{\mathbf{k}_i} + T_i + L_{\omega,N_i} \rightarrow e_{\mathbf{k}_f} + T_i + L_{\omega,N_f}, \tag{1}$$

where $e_{\mathbf{k}_j}$ represents an electron with momentum $\mathbf{k}_j$, L_{ω,N_j} a monochromatic laser field containing N_j photons with energy ω and T_i the unaffected target. Hence, the presence of the field permits processes where $k_i^2 \neq k_f^2$, since by global energy conservation

$$k_f^2 = k_i^2 - 2\ell\omega, \tag{2}$$

with $\ell = N_f - N_i$, the number of photons absorbed ($\ell < 0$) or emitted ($\ell > 0$) by the scattered electron.

The basic task in laser-assisted scattering (LAS) is the determination of the differential cross-section (DCS) for processes involving an exchange of ℓ photons. In the Kroll-Watson approximation (KWA) [1], the DCS associated with the exchange of ℓ photons is expressed by

$$\frac{\mathrm{d}\sigma}{\mathrm{d}\Omega}^{\ell}(\mathbf{k}_f, \mathbf{k}_i) = \frac{k_f}{k_i} J_\ell^2\left(\boldsymbol{\alpha}_0 \cdot (\mathbf{k}_f - \mathbf{k}_i)\right) \frac{\mathrm{d}\sigma^{FF}}{\mathrm{d}\Omega}(\mathbf{K}_f, \mathbf{K}_i), \tag{3}$$

where $J_n(x)$ is an integer-order Bessel function of the first kind, and where the classical quiver radius, expressed in terms of the laser intensity I, $\alpha_0 = \sqrt{I}/\omega^2$, is combined with the polarization vector $\boldsymbol{\varepsilon}$ of the linearly polarized field to give $\boldsymbol{\alpha}_0 = \alpha_0\boldsymbol{\varepsilon}$. The last factor in equation (3) denotes the field-free DCS evaluated at momenta

$$\mathbf{K}_j = \mathbf{k}_j + \boldsymbol{\lambda}, \qquad (j = i, f) \tag{4}$$

with displacement, $\boldsymbol{\lambda}$, given by

$$\boldsymbol{\lambda} = \frac{\ell\omega\boldsymbol{\alpha}_0}{\boldsymbol{\alpha}_0 \cdot (\mathbf{k}_f - \mathbf{k}_i)}. \tag{5}$$

One may verify that $\boldsymbol{K}_i^2 = \boldsymbol{K}_f^2$, so that the KWA is an on-shell approximation.

The experiments by Weingartshofer et al. [2–4] confirmed the qualitative predictions of the KWA, and by including the chaotic laser modes into the KWA, Bivona et al. [5] obtained quantitative agreement. The experiments by Weingartshofer et al. were performed in a geometrical arrangement with $\boldsymbol{\alpha}_0 \parallel (\mathbf{k}_f - \mathbf{k}_i)$, maximizing the argument of the Bessel function in equation (3).

In order to put the KWA to a more critical test Wallbank and Holmes [6] measured the relative laser-assisted signal

$$\mathscr{R}^{\ell} = \frac{\mathrm{d}\sigma^{LA}(\ell)}{\mathrm{d}\sigma^{FF}}, \tag{6}$$

in two critical geometrical arrangements with the laser polarization almost perpendicular to the electron momentum transfer. In one geometry, G_1, the laser polarization is parallel to the direction of the incoming projectile. Consequently, in G_1, the electron momentum transfer is, for photon absorption, perpendicular to $\boldsymbol{\epsilon}$ at the scattering angle $\cos\theta = k_i/k_f$. In the second arrangement, G_2, the laser polarization bisects the scattering angle and $\boldsymbol{\alpha}_0 \cdot (\mathbf{k}_f - \mathbf{k}_i)$

[a] *Present address*: The MR Reseach Centre, Inst. of Exp. Clinical Research, University of Aarhus, Aarhus University Hospital, 8200 Århus N, Denmark.
[b] e-mail: bojer@phys.au.dk

is very close to zero for all scattering angles. According to the KWA, geometries with $\boldsymbol{\alpha}_0 \cdot (\mathbf{k}_f - \mathbf{k}_i) \ll 1$ should produce increasingly small multiphoton signals, and in the strict limit of $\boldsymbol{\alpha}_0 \cdot (\mathbf{k}_f - \mathbf{k}_i) = 0$, only the $\ell = 0$ channel is allowed since $J_\ell(0) = \delta_{\ell,0}$. Experiments, however, showed relative laser-assisted signals several orders of magnitudes larger than predicted by theory [7–10].

Various suggestions to the origin of the discrepancy between experiment and theory have been offered. One being that the KWA breaks down when evaluated in G_1 and G_2. In these cases the displacement vector $\boldsymbol{\lambda}$ of equation (5) may diverge and it was shown in reference [11] that, in addition to the weak-field and soft-photon requirements stipulated in the original paper by Kroll and Watson, the displacement must also be small compared with k_i, $\lambda \ll k_i$, in order for the KWA to be valid. The weak-field soft-photon approximation of reference [11], however, showed no appreciable improvement in terms of agreement with experiment.

Other works [12–14] investigated the importance of the off-shell propagation included in the impulse approximation [1], but ignored in the KWA. The conclusion offered in these publications, however, was that although the off-shell terms may be crucial in certain geometries[1] their inclusion do not explain the experimental findings by Wallbank and Holmes. Another method for including off-shell terms in LAS is the second Born approximation (SBA), originally employed in reference [16]. The only applications of the SBA to date which may be directly compared with experiments are those presented in references [17,18]. Surprisingly, these works reproduced qualitatively the findings of the Wallbank and Holmes experiments. We shall return to these results below.

Finally, calculations including target dressing effects have been performed using, e.g., the Floquet formalism [19,20], R-matrix approach [21] and other dressing techniques [22,23]. Neither of these approaches reproduced the experimental findings.

An alternative hypothesis seems to be that the experimental implementation using a super sonic beam [6] increased the target thickness beyond the point where only single-scattering events contributed to the scattered signal. This was originally proposed in reference [11] and a calculation [24] showed that the KWA could indeed reproduce the general signatures of the experiments with double scattering events included. Nothing conclusive, however, can be said at this point since several unknown experimental parameters had to be modelled [24].

In the present work, we were motivated by the apparently exceptional SBA results reported in references [17,18], to perform a careful comparison between the laser-assisted signals predicted by the SBA and those measured by Wallbank and Holmes. In addition to this comparison, we present an evaluation of the importance of the off-shell propagation of the T-matrix as a function of the range of the scattering potential. In Appendix, we discuss in detail our numerical procedures and the checks we have carried out to be sure of convergence of the results.

[1] For example through the existence of a selection rule when the polarization is perpendicular to the scattering plane [15].

2 Theory

Since the laser field is assumed to be a continuous wave field, the scattering problem may be treated within the stationary T-operator formalism (see, e.g., Ref. [25]), and we have employed a full quantum description of the field in the same manner as presented in reference [26]. Accordingly, the asymptotic scattering states are taken as quantum Volkov states

$$|\,\mathbf{k}; N\,\rangle = |\,\mathbf{k}\,\rangle \otimes \sum_{n=-\infty}^{\infty} J_{-n}(\boldsymbol{\alpha}_0 \cdot \mathbf{k})\,|\,n+N\,\rangle\,, \qquad (7)$$

with $(\,\mathbf{x}\,|\,\mathbf{k}\,) = (2\pi)^{-3/2} e^{-i\mathbf{k}\cdot\mathbf{r}}$ plane wave states, and $|\,n+N\,\rangle$ number states.

The T-matrix in the SBA for the exchange of ℓ photons, is given as

$$T_{fi}^{2.B}(\ell) = T_{fi}^{(1)}(\ell) + T_{fi}^{(2)}(\ell), \qquad (8)$$

with

$$T_{fi}^{(1)}(\ell) = \langle\,\mathbf{k}_f; N_f\,|\,V\,|\,\mathbf{k}_i; N_i\,\rangle\,, \qquad (9)$$

and

$$T_{fi}^{(2)}(\ell) = \langle\,\mathbf{k}_f; N_f\,|\,V \frac{1}{\mathscr{E}_i - \mathscr{H}^0 + i0^+} V\,|\,\mathbf{k}_i; N_i\,\rangle\,, \qquad (10)$$

where V is the potential felt by the electron, $\mathscr{E}_i = k_i^2/2 + N_i\omega$ and $\mathscr{H}^0 = \mathbf{P}^2/2 + \mathbf{A}\cdot\mathbf{P} + \mathbf{N}\omega$, with $\mathbf{A} = A_0(\boldsymbol{\varepsilon} a + \boldsymbol{\varepsilon}^* a^\dagger)/2\sqrt{N}$ and $a, a^\dagger$ annihilation and creation operators and $\mathbf{N} \doteq a^\dagger a$ the number operator. Note that the term quadratic in $\mathbf{A}$ is neglected in $\mathscr{H}^0$. This amounts to neglecting the ponderomotive correction to the energy [11, 26], which for the parameters relevant to the Wallbank and Holmes experiments is on the order of $\omega/100$.

With the T-matrix at hand, and the $(2\pi)^{-3/2}$ normalization of the Volkov waves, the DCS reads

$$\frac{\mathrm{d}\sigma^\ell}{\mathrm{d}\Omega}((\mathbf{k}_f, \mathbf{k}_i) = \frac{k_f}{k_i}(2\pi)^4 |T_{fi}(\ell)|^2. \qquad (11)$$

The individual matrix elements of equation (8) may be evaluated by exploiting completeness

$$\int \mathrm{d}\boldsymbol{\kappa} \sum |\,\boldsymbol{\kappa}; N\,\rangle\,\langle\,\boldsymbol{\kappa}; N\,| = \mathbb{I}, \qquad (12)$$

orthonormality

$$\langle\,\boldsymbol{\kappa}; N\,|\,\boldsymbol{\zeta}; M\,\rangle = \delta_{N,M}\delta(\boldsymbol{\zeta} - \boldsymbol{\kappa}), \qquad (13)$$

and the addition formula (see, e.g., Ref. [27])

$$\sum_{k=-\infty}^{\infty} J_{n\mp k}(\eta) J_k(\zeta) = J_n(\eta \pm \zeta), \quad n \in \mathbb{Z}. \qquad (14)$$

For $T_{fi}^{(1)}(\ell)$, we regain the first Born approximation (FBA) result of Bunkin and Federov [28]

$$T_{fi}^{(1)}(\ell) = (-1)^{-\ell}\widetilde{V}_{fi}J_\ell(\boldsymbol{\alpha}_0 \cdot (\mathbf{k}_f - \mathbf{k}_i)), \qquad (15)$$

with $\widetilde{V}_{fi}$ the Fourier transform of the scattering potential. For the second amplitude, we find

$$T_{fi}^{(2)}(\ell) = (-1)^{\ell} \sum_{N=-\infty}^{\infty} \int \mathrm{d}\boldsymbol{\kappa}\, T_{f\kappa}^{(1)}(\ell - N) \times \frac{-2}{\kappa^2 - \rho_N^2 - i0^+} T_{\kappa i}^{(1)}(N), \qquad (16)$$

where $\rho_N^2 = k_i^2 - 2N\omega$. For the atomic potential, we follow references [17,18] and use

$$V(\mathbf{r}) = \frac{Z}{r}\sum_{j=1}^{n} A_j e^{-\mu_j r}, \qquad (17)$$

with Z the atomic number, A_i the 'strength' of the potential and μ_i the inverse range. The parameters A_i and μ_j were calculated in reference [29], and the sum contains 2 and 3 terms in the cases of He and Ar, respectively. The Fourier transform of this potential is obtained in analytical form

$$\tilde{V}_{\kappa\kappa'} = Z\frac{-4\pi}{(2\pi)^3}\sum_{j=1}^{n}\frac{A_j}{\mu_j^2 + |\boldsymbol{\kappa} - \boldsymbol{\kappa}'|^2}. \qquad (18)$$

3 Results and discussion

We have performed a number of different calculations using the methods and numerical parameters described in Appendix. We have put special emphasis on the question of convergence, and found, for example, that one needs to retain as many as ∼120 virtual photon exchanges in equation (16) to obtain a reasonably degree of convergence.

Considering that the experiments [6–10] measured the relative laser-assisted signals directly, we base the comparison with experiment on the relative signals only. For consistency, the relative laser-assisted signals are produced using the SBA field-free DCS rather than a partial wave DCS. A detailed comparison between the differential cross-sections for electron-He and -Ar scattering, calculated using the partial wave, first and second Born approximation and the [1,1]-Padé approximant methods was given in reference [30]. The FBA-, SBA- and [1,1]-Padé-DCS's are calculated using the relevant potential parameters proposed in references [12,29]. In reference [30] it was shown that the SBA overestimates the DCS when calculated with the parameters for Ar from reference [29] by as much as two orders of magnitude. This means that the relative laser-assisted signal (6) if taken as the ratio between the SBA LAS DCS and the exact result would produce artificially large relative signals [17,18].

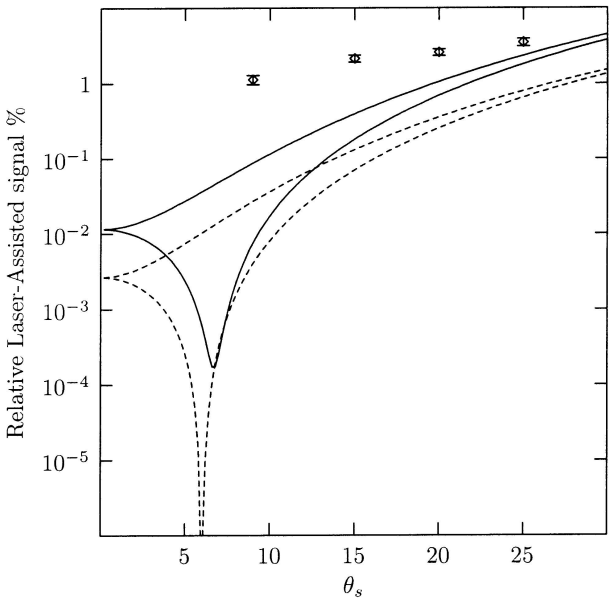

Fig. 1. Relative laser-assisted signals for e-He scattering in the G_1-geometry with $E_i = 10.5$ eV and for 1-photon exchange. The curves with dips around 6−7° correspond to absorption. The curves without dips to emission. (⊞) Experimental data from reference [31]; (- - - -) FBA; (——) SBA.

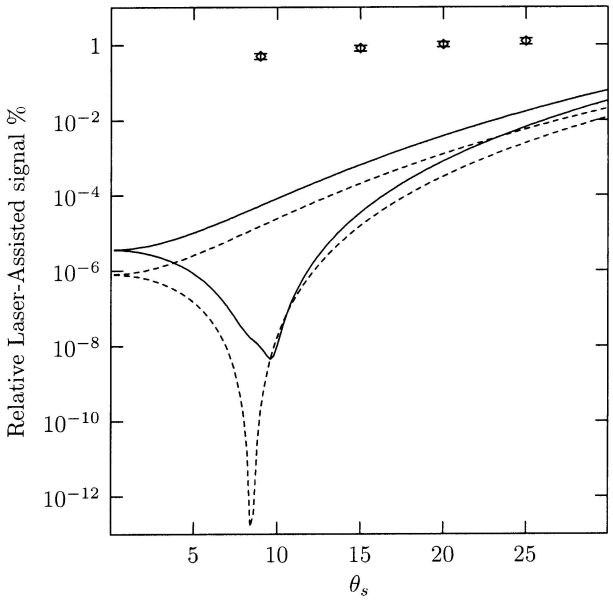

Fig. 2. As Figure 1, but for 2-photon absorption.

Figures 1–3 show the FBA and the SBA relative laser-assisted signal for electron-He scattering in the G_1 arrangement with the laser polarization parallel with the momentum of the incoming electron. The projectile energy is 10.5 eV, and the scattering potential parameters are those proposed in reference [29] in all three figures. We register only marginal improvement of the SBA over the FBA in terms of agreement with experiment. Both the FBA and the SBA, contrary to the Born results of

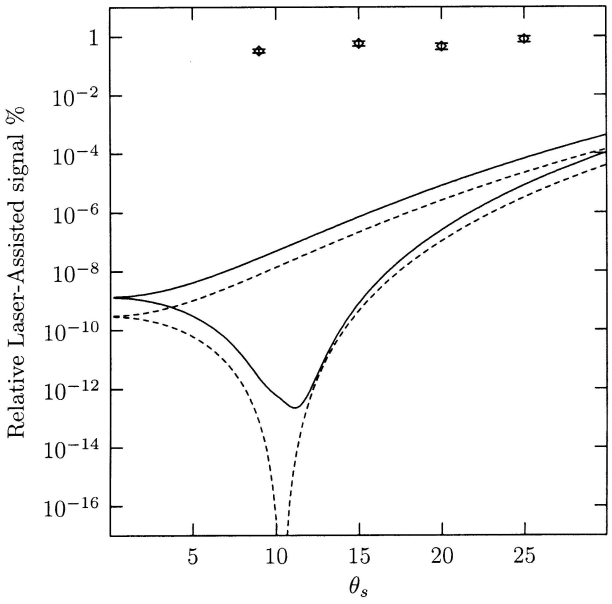

Fig. 3. As Figure 1, but for 3-photon absorption.

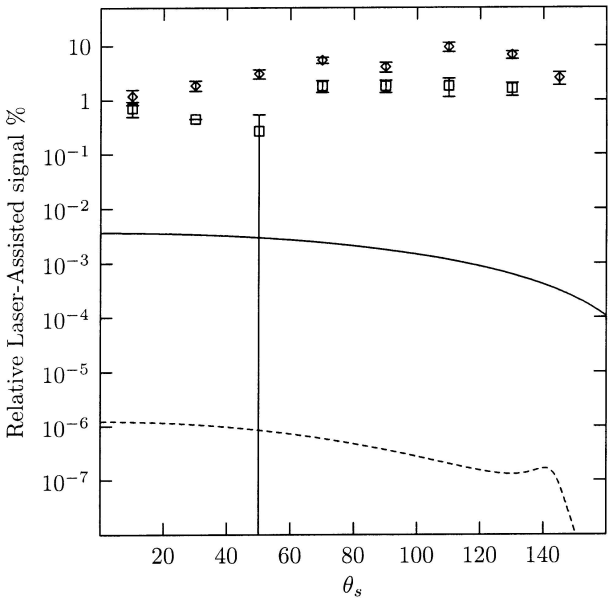

Fig. 4. Relative laser-assisted signal for e-Ar scattering in the G_2-geometry with $E_i = 8$ eV. Data points from reference [8]. (⊕) 1-photon absorption; (⊞) 2-photon absorption; (——) SBA 1-photon absorption; (- - - -) SBA 2-photon absorption. Note the datapoint at 50°. Here the measured laser-assisted signal minus the errorbar taken from reference [8] is zero and it is a consequence of the logarithmic scale that the errorbar looks as it does.

reference [17], display distinct dips in the vicinity of the critical geometry. The general impression conveyed by the results is that the discrepancy between theory and experiment at small angles increases with increasing photon exchange, similar to what is predicted by the KWA.

Figures 4 and 5 display the FBA and SBA relative laser-assisted signals for electron-Ar scattering at projectile energies of 8 eV and 20 eV, respectively. The scattering potential parameters are those proposed in reference [12]. The geometric arrangement is G_2 with the laser polarization bisecting the electron scattering angle. As in the previous case, we have not been able to reproduce the experimental findings. The relevant signals are several orders of magnitude smaller than found by experiment. Furthermore the relative difference between the theoretical one- and two-photon signals is far greater than the corresponding experimental difference.

The obstacle in evaluating the SBA T-matrix is the $T_{fi}^{(2)}(\ell)$ term of equation (16). Inserting equation (18) into equation (16), we find

$$T_{fi}^{(2)}(\ell) \propto \sum_{N=-\infty}^{\infty} \sum_{l=1}^{n} \sum_{j=1}^{n} A_l A_j \mathscr{T}(\mathbf{k}_i, \mu_j; \mathbf{k}_f, \mu_l; N), \quad (19)$$

and the problem is reduced to the evaluation of integrals of the type

$$\mathscr{T}(\mathbf{k}_i, \mu_j; \mathbf{k}_f, \mu_l; N) = \int \frac{\mathrm{d}\boldsymbol{\kappa}}{\kappa^2 - \rho_N^2 - i0^+} \times \frac{J_{\ell-N}(\boldsymbol{\alpha}_0 \cdot (\mathbf{k}_f - \boldsymbol{\kappa}))}{\mu_l^2 + |\mathbf{k}_f - \boldsymbol{\kappa}|^2} \frac{J_N(\boldsymbol{\alpha}_0 \cdot (\boldsymbol{\kappa} - \mathbf{k}_i))}{\mu_j^2 + |\boldsymbol{\kappa} - \mathbf{k}_i|^2}. \quad (20)$$

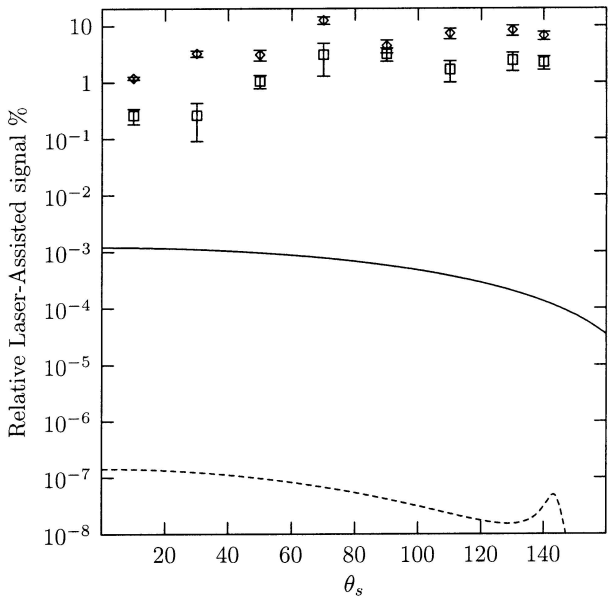

Fig. 5. As Figure 4 but for $E_i = 20$ eV.

An analytical expression for this integral does not exist. If, however, the dependence of the summation index of the denominator is neglected, the integral can be closed by eliminating the Bessel functions using the addition formula (14). This problem was already treated in reference [32], where the authors introduced a mean value

$\rho_{\overline{N}}$ so that

$$\sum_{N=-\infty}^{\infty} \mathscr{T}(\mathbf{k}_i, \mu_j; \mathbf{k}_f, \mu_l; N) = J_\ell(\boldsymbol{\alpha}_0 \cdot (\mathbf{k}_f - \mathbf{k}_i)) \times \mathscr{L}(\mathbf{k}_i, \mu_j; \mathbf{k}_i, \mu_l; -i\rho_{\overline{N}}), \quad (21)$$

where $\mathscr{L}$ is the solution to the so-called Lewis integral [33]

$$\mathscr{L}(\mathbf{k}_i, \mu_1; \mathbf{k}_f, \mu_2; \lambda) = \int \frac{\mathrm{d}\boldsymbol{\kappa}}{(\mu_1^2 + |\boldsymbol{\kappa} - \mathbf{k}_i|^2)(\kappa^2 + \lambda^2)(\mu_2^2 + |\mathbf{k}_f - \boldsymbol{\kappa}|^2)}, \quad (22)$$

which has received extensive treatments (see, e.g., Refs. [34,35] and references therein).

Although providing information of the mean off-shell propagation the practical use of the parameter $\rho_{\overline{N}}$ is rather limited since its determination would require evaluating the integral numerically and subsequently employing some minimization routine to find $\overline{N}$. The precision of $\overline{N}$ would thus be highly dependent on the precision of the integration technique employed. Furthermore, as will become apparent below, the parameter is a function of both scattering angle, ℓ and most likely E_i. For these reasons, we aim, in the present case, at a precise calculation of $T^{(1)}(\ell)$ and $T^{(2)}(\ell)$ as they stand. As a limiting case, we investigate the on-shell approximation

$$\omega \ll k_i \Rightarrow \rho_N \simeq k_i. \quad (23)$$

This will facilitate an investigation into the importance of the off-shell propagation. As a quantitative measure of this effect, we shall consider the relative deviation between the off-shell and on-shell second Born (2B) signals

$$\mathscr{R} = \left| \frac{\mathrm{d}\sigma^{2B} - \mathrm{d}\sigma^{2B}(\rho_N = k_i)}{\mathrm{d}\sigma^{2B}} \right|. \quad (24)$$

Figure 6 shows this deviation in the G_1 geometry with parallel polarization and incoming momentum. From the figure, we see that the effects of off-shell propagation, as maintained in the SBA, are largest at a scattering angle of around 10°, corresponding to the situation where the electron momentum transfer vector is perpendicular to the polarization vector of the field. The different curves show deviations for different ranges of the atomic potential $Ae^{-2\mu r}/r$ with $A = 2$ and μ specified in the figure caption. The smaller the value of μ, the longer the range of the potential. As seen from the figure, the angular window in which the off-shell propagation is significant broadens with the potential range, in accordance with the fact that no off-shell effects are present in the case of a zero-range potential [13]. The relative deviation at angles larger than 15° may be associated with the numerical precision of the SBA rather than with the importance of off-shell propagation.

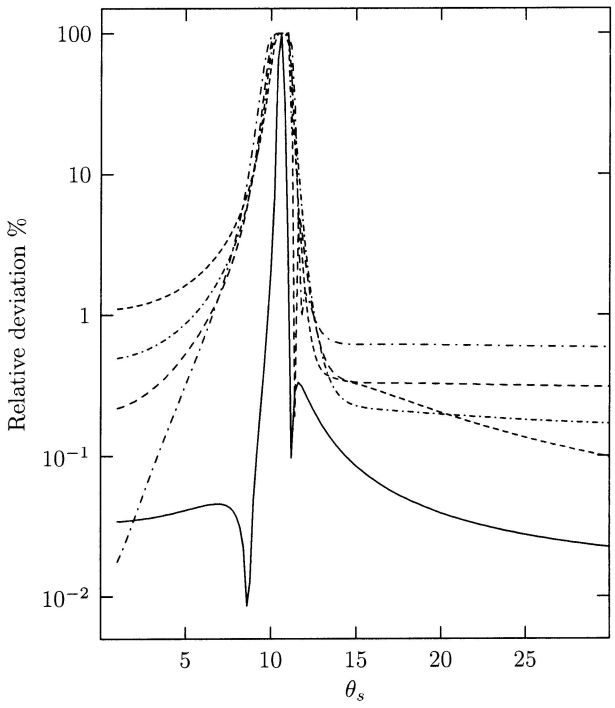

Fig. 6. The relative deviation, equation (24), between the 'exact' off-shell SBA DCS and the on-shell approximation for 3-photon absorption in G_1, $E_i = 10$ eV. (——) $\mu = 5.00$ a.u.; (- - - -) $\mu = 1.00$ a.u.; (— —) $\mu = 0.20$ a.u.; (-·-) $\mu = 0.10$ a.u.; (– · –) $\mu = 0.05$ a.u.

4 Conclusion

The present work was motivated by the results published in references [17,18] where the authors claimed to have obtained good agreement with the experiments of Wallbank and Holmes by doing calculations in the laser-assisted second Born approximation. Considering that more elaborate theories had failed in this quest [19,20], the good agreement with the SBA results came as a surprise to us. In this work therefore, we reexamined in detail the second Born approximation for laser-assisted charged-particle scattering. To make possible an assessment of the quality of our calculations and in view of the results referred to above, we have discussed in some detail our numerical procedures and the tests we have made of convergence in Appendix. Within the accuracy of our calculations, we find an effect of the off-shell propagation. In particular, in the critical geometries with nearly orthogonal laser polarization vector and electron momentum transfer, the off-shell-propagation is important. In contrast to the works [17,18], however, we do not obtain any significant improvement in the comparison with the experimental results. Our results are orders of magnitude smaller. Accordingly, we conclude, that despite intense theoretical efforts no theory has been able to explain satisfactorily the experimental results of Wallbank and Holmes [7,8]. One exception being the calculations of Rabadán and Dickinson [24] assuming a double scattering mechanism.

SH gratefully acknowledges the helpful correspondence with Prof. D. Belkić. LBM acknowledges support from the Danish Natural Science Research Council (Grant No 21-03-0163).

Appendix

The numerical evaluation of the SBA matrix elements is complicated by a number of different factors. A suitable cutoff needs to be found for the number of terms included in the infinite sum over N, as well as for the upper boundary for the radial integration over κ in equation (16). In addition, the singular and rapidly oscillating nature of the integrand needs special attention.

We have chosen to evaluate the matrix elements in spherical coordinates, and subsequently arranging the reference frame so that the polar axis is parallel to the laser polarization $\boldsymbol{\varepsilon}$. This avoids any azimuthal dependency of the Bessel functions so that the azimuthal integral may be performed analytically. The remaining two-dimensional integral is performed as a series of one-dimensional Gauss-Legendre quadratures, with the radial part needing special treatment in accordance with the issues raised above.

In evaluating the remaining integrals, we note that

$$\frac{1}{\kappa^2-\rho_N^2-i\epsilon} \underset{\epsilon\to 0}{\sim} \frac{1}{\kappa+\rho_N}\frac{1}{\kappa-\rho_N-i\epsilon}, \tag{25}$$

which permits to use

$$\lim_{\epsilon\to 0^+}\frac{1}{\kappa-\rho_N-i\epsilon} = \mathscr{P}\frac{1}{\kappa-\rho_N}+i\pi\delta\left(\kappa-\rho_N\right). \tag{26}$$

We absorb the polar integral as well as the regular portion of the radial integrand into the function $\Theta(\kappa)$, and cast the reduced matrix element (20) into the form

$$\begin{aligned}\mathscr{T} &= \int_0^\infty \mathrm{d}\kappa\left\{\mathscr{P}\frac{1}{\kappa-\rho_N}+i\pi\delta\left(\kappa-\rho_N\right)\right\}\Theta(\kappa)\\ &= \not\int_0^\infty \mathrm{d}\kappa\frac{\Theta(\kappa)}{\kappa-\rho_N}+i\pi\Theta(\rho_N).\end{aligned} \tag{27}$$

In order to perform the Cauchy Principal Value (CPV) integral

$$\mathscr{T}^{cpv} = \not\int_0^\infty \mathrm{d}\kappa\frac{\Theta(\kappa)}{\kappa-\rho_N} \tag{28}$$

we follow reference [36], and divide the interval of integration into three parts

$$\mathscr{T}^{cpv} = \not\int_{\rho_N-\Delta}^{\rho_N+\Delta}\mathrm{d}\kappa\frac{\Theta(\kappa)}{\kappa-\rho_N}+\mathscr{I}^0, \tag{29}$$

where $\mathscr{I}^0$ is the remainder of the integral (28), and Δ is a suitably chosen cutoff, which determines the degree to which the limiting process, inherent to the CPV integral, is approximated. The CPV integral may subsequently be regularized by an on-shell subtraction

$$\not\int_{\rho_N-\Delta}^{\rho_N+\Delta}\mathrm{d}\kappa\frac{\Theta(\kappa)}{\kappa-\rho_N} = \not\int_{-1}^{1}\mathrm{d}\kappa\frac{\Theta(\kappa\Delta+\rho_N)-\Theta(\rho_N)}{\kappa}. \tag{30}$$

Assuming that $\Theta(\kappa)$ is a continuously differentiable function, the resulting regular integral can be evaluated by an even-order quadrature rule that distributes the abscissae symmetrically about the origin. In the present case, we have employed an 8-order Gauss-Legendre quadrature rule.

The primary purpose of the calculations to be presented has been to perform a qualitative comparison with experimental data. Hence we have chosen to accept relative numerical errors on the order of 10%, in the interest of retaining an acceptable level of computational time consumption. Our investigations have shown that the number of terms retained in the sum over virtual photon exchanges may dramatically influence the convergence of the matrix element.

The assessment of numerical parameters is greatly simplified by the existence of the somewhat similar Lewis integral (22), introduced in connection with the closure approximation in Section 3

$$\begin{aligned}\mathscr{I} &= \sum_{N=-\infty}^{\infty}\int\frac{\mathrm{d}\boldsymbol{\kappa}}{k^2-\rho^2-i0^+}\\ &\quad\times\frac{J_{\ell-N}(\boldsymbol{\alpha}_0\cdot(\mathbf{k}_f-\boldsymbol{\kappa}))}{\mu_1^2+\left|\mathbf{k}_f-\boldsymbol{\kappa}\right|^2}\frac{J_N(\boldsymbol{\alpha}_0\cdot(\boldsymbol{\kappa}-\mathbf{k}_i))}{\mu_2+\left|\boldsymbol{\kappa}-\mathbf{k}_i\right|^2}\\ &= J_\ell(\boldsymbol{\alpha}_0\cdot(\mathbf{k}_f\mathbf{k}_i))\mathscr{L}(\mathbf{k}_i,\mu_1;\mathbf{k}_f,\mu_2;-i\rho).\end{aligned} \tag{31}$$

We have found that the choice of the cutoff Δ, introduced in equation (29), does not critically influence the general level of numerical precision, and we use the value $\Delta = 0.05\rho_N$ throughout. Furthermore, comparison between numerical and analytical evaluations of the Lewis integral (22) has shown that choosing a radial cutoff of $\kappa_{max} = 10$ a.u. will produce a relative error ∼0.7%. We have used this κ_{max} for all calculations.

Turning now to the determination of the summation cutoff in N, N_{max}, we recall the behavior of non-zero order Bessel functions at arguments much less than their order. These functions decrease to zero and it is clear that the finite value of the radial cutoff sets a limit to the number of terms which contribute to the integral. Thus the value of κ_{max} has been chosen such that a sufficient number of terms in the sum may be included to ensure proper convergence of the matrix elements. To quantify this point, we calculate the on-shell approximation with closure (31) and compare this with a numerical calculation of the same quantity. Figures 7 and 8 display the relative error of this numerical result

$$\mathscr{R}(N_{max}) = \left|\frac{\mathrm{d}\sigma(\mathscr{I})-\mathrm{d}\sigma(Q(\mathscr{I}))}{\mathrm{d}\sigma(\mathscr{I})}\right|, \tag{32}$$

where $Q(\mathscr{I})$ represents the applied quadrature technique for a different number of terms included in the 'infinite' sum. For these calculations we have used

$$V(r) = \frac{e^{-2r}}{r}, \tag{33}$$

for the scattering potential and a projectile energy of 10 eV. Laser parameters are identical to those employed by Wallbank and Holmes, i.e., $\omega = 0.117$ eV and $\alpha_0 = 3.5$ a.u. Figures 7 and 8 reveal that precision is far better when

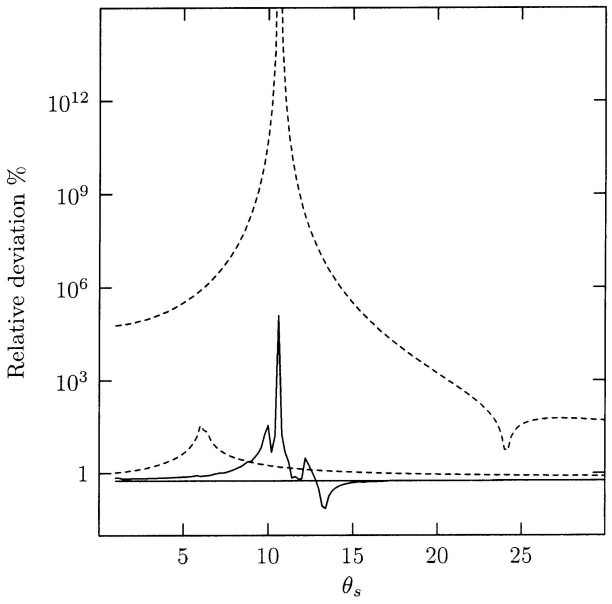

Fig. 7. The relative deviation introduced in equation (32) with $\ell = -1, -3$ in G_1. (——) $N_{max} = 60$; (- - - -) $N_{max} = 15$. Higher relative errors for similar line types correspond to higher values of ℓ.

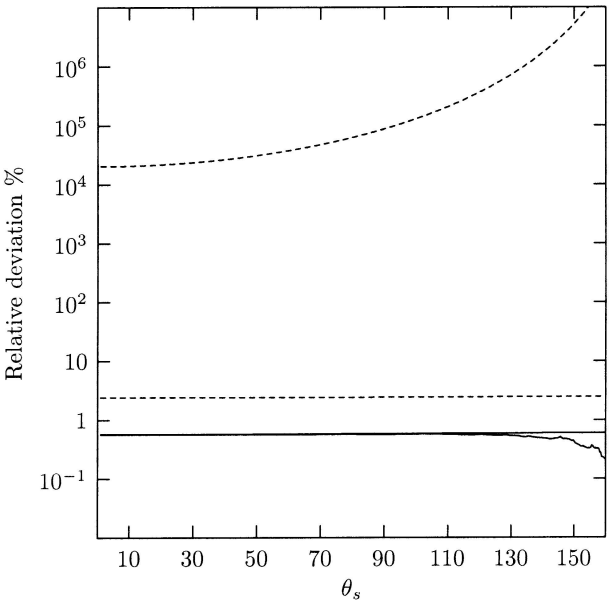

Fig. 8. Relative deviation as in Figure 7 but in the G_2 geometry, and for $\ell = 1, 2$.

including 121 terms ($N_{max} = 60$) than when including only 31 terms ($N_{max} = 15$). The effect is especially pronounced for photon exchanges > 1, rendering calculations based on $N_{max} = 15$ highly inaccurate over a rather wide angular window around the critical geometry. This means that calculations in the G_2 arrangement are especially dependent on the choice of N_{max} since the critical geometry stretches over the entire range of the plot. This is emphasized by Figure 8, where the $\ell = 1, 2$ relative deviations for $N_{max} = 60$ cannot be resolved from one another except for $\theta_s \geq 110°$ where the $\ell = 2$ signal improves in terms of accuracy. The corresponding relative deviations for $N_{max} = 15$ differ by several orders of magnitude.

Our investigations have showed that a further increase in the number of included terms will not improve precision if the present value of $\kappa_{max} = 10$ a.u. is to be retained. Hence, we may regard the relative error associated with $N_{max} = 60$ as a minimum at the current value of κ_{max}. Furthermore our investigations have showed that increasing the value of κ_{max} even only by a factor of 2 will greatly complicate numerical procedures and increase the required number of quadrature points dramatically. Finally, it should be noted that the precision associated with a given set of numerical parameters will depend on the range of the potential (33) as discussed in Section 3 in connection with Figure 6.

References

1. N.M. Kroll, K.M. Watson, Phys. Rev. A **8**, 804 (1973)
2. A. Weingartshofer, J.K. Holmes, G. Caudle, E.M. Clarke, H. Krüger, Phys. Rev. Lett. **39**, 269 (1977)
3. A. Weingartshofer, E.M. Clarke, J.K. Holmes, C. Jung, Phys. Rev. A **19**, 2371 (1979)
4. A. Weingartshofer, J.K. Holmes, J. Sabbagh, S.L. Chin, J. Phys. B: At. Mol. Phys. **16**, 1805 (1983)
5. S. Bivona, R. Burlon, R. Zangara, G. Ferrante, J. Phys. B: At. Mol. Phys. **18**, 3149 (1985)
6. B. Wallbank, J.K. Holmes, Phys. Rev. A **48**, R2515 (1993)
7. B. Wallbank, J.K. Holmes, J. Phys. B: At. Mol. Opt. Phys. **27**, 1221 (1994)
8. B. Wallbank, J.K. Holmes, J. Phys. B: At. Mol. Opt. Phys. **27**, 5405 (1994)
9. B. Wallbank, J.K. Holmes, J. Phys. B: At. Mol. Opt. Phys. **29**, 5881 (1996)
10. B. Wallbank, J.K. Holmes, Can. J. Phys. **79**, 1237 (2001)
11. L.B. Madsen, K. Taulbjerg, J. Phys. B: At. Mol. Opt. Phys. **28**, 5327 (1995)
12. D.B. Milošević, F. Ehlotzky, J. Phys. B: At. Mol. Opt. Phys. **30**, 2999 (1997)
13. L.B. Madsen, K. Taulbjerg, J. Phys. B: At. Mol. Opt. Phys. **31**, 4701 (1998)
14. L.W. Garland, A. Jaroń, J.Z. Kamiński, R.M. Potvliege, J. Phys. B: At. Mol. Opt. Phys. **35**, 2861 (2002)
15. L.B. Madsen, A. Jaroń, J.Z. Kamiński, K. Taulbjerg, Phys. Rev. A **60**, 5126 (1999)
16. F. Trombetta, G. Ferrante, J. Phys. B: At. Mol. Opt. Phys. **22**, 3881 (1989)
17. J. Sun, S. Zhang, Y. Jiang, G. Yu, Phys. Rev. A **58**, 2225 (1998)
18. S. Zhang, X. Qian, Y. Jiang, J. Sun, Chin. Phys. Lett. **17**, 496 (2000)
19. N.J. Kylstra, C.J. Joachain, Phys. Rev. A **58**, 26 (1998)
20. N.J. Kylstra, C.J. Joachain, Phys. Rev. A **60**, 2255 (1999)
21. M. Terao-Dunseath, K.M. Dunseath, J. Phys. B: At. Mol. Opt. Phys. **35**, 125 (2002)
22. M. Bouzidi, A. Makhoute, D. Khalil, A. Maquet, C.J. Joachain, J. Phys. B: At. Mol. Opt. Phys. **34**, 737 (2001)
23. A. Makhoute, D. Khalil, M. Zitane, M. Bouzidi, J. Phys. B: At. Mol. Opt. Phys. **35**, 957 (2002)

24. I. Rabadán, L. Méndez, A.S. Dickinson, J. Phys. B: At. Mol. Opt. Phys. **29**, L801 (1996)
25. J.R. Taylor, *Scattering Theory: The Quantum Theory on Nonrelativistic Collisions* (John Wiley & Sons, New York, 1972)
26. E.J. Kelsey, L. Rosenberg, Phys. Rev. A **19**, 756 (1979)
27. M. Abramowitz, I.A. Stegun, *Handbook of Mathematical Functions*, 6th edn. (Dover, Washington, 1967)
28. F.V. Bunkin, M.V. Fedorov, Sov. Phys. JETP **22**, 844 (1966)
29. F. Salvat, J.D. Martínez, R. Mayol, J. Parellada, Phys. Rev. A **36**, 467 (1987)
30. S.L. Hokland, Master's thesis, Department of Physics, University of Aarhus (2003)
31. B. Wallbank, *Laser-Assisted Electron-Atom Collisions* (AIP Conf. Proc., 1995), Vol. 360
32. F. Trombetta, Phys. Rev. A **43**, 6401 (1991)
33. R.R. Lewis Jr, Phys. Rev. **102**, 537 (1956)
34. D. Belkić, Z. Phys. A **317**, 131 (1984)
35. U. Roy, N.C. Sil, J. Phys. B: At. Mol. Opt. Phys. **30**, 3423 (1997)
36. J.V. Noble, Comput. Sci. Engineer. **2**, 92 (2000)